SCIENTIFIC REPORTS

Corrected: Author Correction

OPEN

All-optical implementation of collision-based evolutions of open quantum systems

Received: 18 September 2018
Accepted: 25 January 2019
Published online: 01 March 2019

Álvaro Cuevas[1], Andrea Geraldi[1], Carlo Liorni[1,2], Luís Diego Bonavena[1], Antonella De Pasquale[3,4], Fabio Sciarrino[1], Vittorio Giovannetti[5] & Paolo Mataloni[1]

We present a new optical scheme enabling the implementation of highly stable and configurable non-Markovian dynamics. Here one photon qubit can circulate in a multipass bulk geometry consisting of two concatenated Sagnac interferometers to simulate the so called collisional model, where the system interacts at discrete times with a vacuum environment. We show the optical features of our apparatus and three different implementations of it, replicating a pure Markovian scenario and two non-Markovian ones, where we quantify the information backflow by tracking the evolution of the initial entanglement between the system photon and an ancillary one.

Precise control of quantum states is a crucial requirement for future quantum technologies[1,2]. Their processing protocols should preserve and distribute microscopic correlations in macroscopic scenarios, where countable quantum systems are subjected to environmental noise. It is essential in this context to understand how much robust are the possible quantum dynamical processes and the best way to control the information permeability between the systems and their environment[3–8].

Quantum dynamical processes do not act merely on the sample system, actually they act in an extended Hilbert space where system and its surrounding environment are in contact[9,10]. The non-isolated sample system s is called *open quantum system* (OQS), and is characterized by a state $\rho_s \in \mathcal{H}_s$. Similarly, the environment e is characterized by a state $\rho_e \in \mathcal{H}_e$. Without loss of generality, one can assume that the extended system $s-e$ that lives in $\mathcal{H} = \mathcal{H}_s \otimes \mathcal{H}_e$ is closed, then no information can be lost but only distributed inside $\mathcal{H}$[11,12].

The dynamics of an OQS are called Markovian if each continuous or discrete section of the total evolution is independent of the previous ones, otherwise they are called non-Markovian[13]. In the quantum scenario, three different approaches are widely used to quantify the degree of non-Markovianity of a process[14,15]. The first method is based on the presence of information back-flow towards the system from the environment, that acts in this case as a reservoir of information[16–18]. In the OQS framework the total system-environment state $\rho_{s,e} \in \mathcal{H}$ evolves according to a quantum process generating a communication link between $\mathcal{H}_s$ and $\mathcal{H}_e$. Here the strength of the flow of information between system and environment during their interaction can be used to discriminate the level of non-Markovianity of the process. The second approach studies the divisibility of the process in *Completely Positive* (CP) maps, defining the evolution as non-Markovian if this decomposition fails at some time[14,19]. In cases were this CP divisibility is valid, also master equations can be well defined[20]. The third method, which has been used in this work, studies the evolution of the entanglement between the system and an isolated ancilla and it is strictly related to the two approaches mentioned above. In order to explain it we refer to the next section and to[14,21].

If the environment is represented by an ensemble of spaces $\mathcal{H}_e = \mathcal{H}_{e_1} \otimes \ldots \otimes \mathcal{H}_{e_k}$, and the system space $\mathcal{H}_s$ interacts sequentially with each of them at discrete times, we obtain the so called *collisional model* (CM)[22–26]. It represents a powerful tool to approximate continuous-time quantum dynamics and to analyze non-Markovian dynamics of OQSs[27–32]. Linear optics platforms have been thoroughly analyzed for the implementation of

[1]Department of Physics, University of Rome La Sapienza, Piazzale Aldo Moro 5, 00185, Rome, Italy. [2]Heinrich-Heine Universität, Institut für Theoretische Physik III, Universitätstraße 1, 40225, Düsseldorf, Germany. [3]Department of Physics, University of Florence, Via G. Sansone 1, I-50019, Sesto Fiorentino, Florence, Italy. [4]INFN Sezione di Firenze, Via G. Sansone 1, I-50019, Sesto Fiorentino, Florence, Italy. [5]NEST, Scuola Normale Superiore and Istituto Nanoscienze, Piazza dei Cavalieri 7, 56126, Pisa, Italy. Correspondence and requests for materials should be addressed to Á.C. (email: alvaro.cuevas@uniroma1.it) or V.G. (email: vittorio.giovannetti@sns.it) or P.M. (email: paolo.mataloni@uniroma1.it)

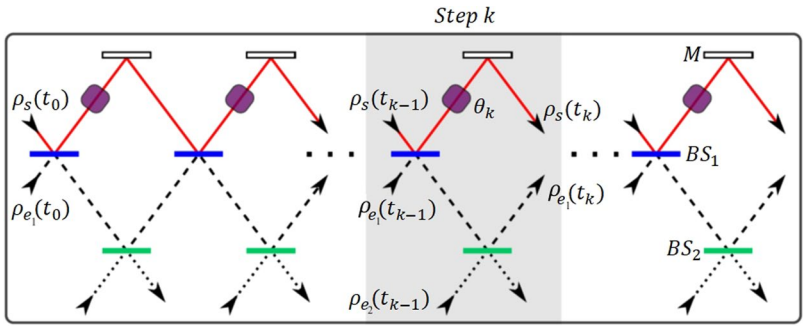

Figure 1. Linear optics scheme for the CM: Each step-k begins with the $s-e_1$ collision in BS_1 (in blue) and it ends with the e_1-e_2 collision in BS_2 (in green). The phase factor θ_k mediates the collision of the step-(k + 1) by optical interference.

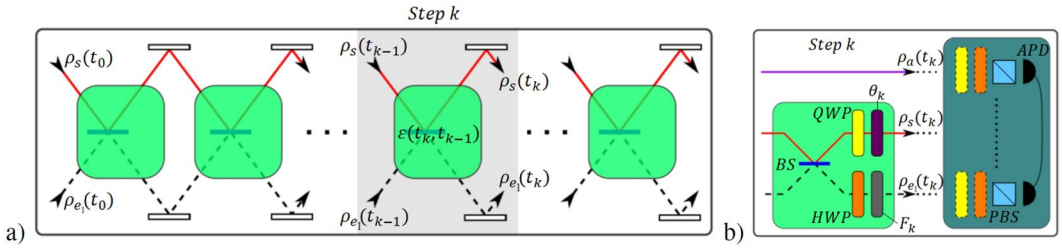

Figure 2. Proposed optical scheme, alternative to the one of Fig. 1: (**a**) When $r_2 = 1$ each BS_2 is replaced by a perfect mirror M. The system-environment collision occurs when $\rho_s(t_{k-1})$ interferes with $\rho_{e_1}(t_{k-1})$ inside the green box associated to $\varepsilon(t_k, t_{k-1})$. (**b**) The green boxes include a BS, a QWP and a phase factor θ_k in the s-mode and a HWP and a filter F_k in the e_1-mode. The environment memory is controlled by F_k, while θ_k mediates the collision of the step-(k + 1) as in the original CM. Two-qubit polarization tomographies can be measured between a-s modes or a-e_1-modes[52] by registering the photon coincidences between two *avalanche photodetectors* (*APDs*) after a series of polarization projections through a *polarizing beam splitter* (*PBS*).

CMs[33,34]. A simple and effective implementation has been proposed by some of us[35]. There the authors consider an initial photon state $\rho_s(t_0) \in \mathcal{H}_s$, whose spatial mode collides sequentially with the modes of an environment ensemble, which can be considered as a double space environment $\mathcal{H}_e = \mathcal{H}_{e_1} \otimes \mathcal{H}_{e_2}$ with one subspace always prepared in a certain generic state $\rho_{e_2} \in \mathcal{H}_{e_2}$ at any step-k of the process. The evolution of $\rho_s(t_k)$ is mainly controlled by the interaction involving the Hilbert spaces $\mathcal{H}_s$ and $\mathcal{H}_{e_1}$, while the memory effects are due to the inter-environment collisions written in $\mathcal{H}_{e_1}$ and $\mathcal{H}_{e_2}$, which also produces an effective evolution in $\rho_{e_1}(t_k) \in \mathcal{H}_{e_1}$.

The optical implementation described in[35] is realized by a sequence of *Mach-Zehnder interferometers* (*MZIs*) as shown in Fig. 1, where the continuous trajectory is associated to ρ_s, the segmented trajectories to ρ_{e_1} and the dotted trajectory to ρ_{e_2}. At the step-k of this process $\rho_s(t_{k-1})$ interferes with $\rho_{e_1}(t_{k-1})$ in the *beam splitter* BS_1, while the inter-environment collision with ρ_{e_2} occurs in BS_2, which posses a variable reflectivity $R_{BS} \in [0, 1]$ to control the environment memory.

Theoretical Model

In our proposal (shown in Fig. 2a) we consider that all BS_2 have reflectivity $r_2 = 1$, so that they can be substituted with *perfectly reflective mirrors* (*M*). Here the continuous trajectories correspond to the system (*s*-mode) while the segmented ones correspond to the first environment subspace (e_1-mode), as in Fig. 1. However, the second environment subspace (e_2-mode) has no defined path (not present in Fig. 2), since it represents the "absorption environment" after the action of a polarization independent neutral filter F_k placed in the e_1-mode. As seen in Fig. 2b, the super-operator process $\varepsilon(t_k, t_{k-1})$ is composed by a *quarter wave plate* (*QWP*) in the *s*-mode and a *half wave plate* (*HWP*) in the e_1-mode, both at fixed rotation angle $\phi = 0$. The environment memory is controlled by the transmissivity factor $T_k \in [0, 1]$ of F_k, which gives access to the vacuum state stored by $\rho_{e_2} = |0\rangle\langle 0|$, hence effectively mimicking the interaction with the dotted-lines of Fig. 1. The phase factor θ_k mediates collision mechanism by controlling the optical interference. Accordingly, in this setting a purely Markovian dynamics corresponds to the minimum information backflow from $\mathcal{H}_{e_1}$ to $\mathcal{H}_s$, which is achieved by the maximum loss of information from $\mathcal{H}_{e_1}$ to $\mathcal{H}_{e_2}$ ($T_k = 0$). Non-Markovian dynamics instead can arise whenever using $T_k \neq 0$. Let us suppose that the s-mode is initially prepared in a maximally entangled state with an external ancillary system (a-mode) as $|\Psi^{\pm}_{a,s}\rangle = \frac{1}{\sqrt{2}}(|H\rangle_a|V\rangle_s \pm |V\rangle_a|H\rangle_s)$, where $|H\rangle$ ($|V\rangle$) represents the horizontal (vertical) polarization of a photon

qubit. Since both e-modes are initialized in a vacuum state $|0\rangle$, the actual complete initial state corresponds to $\rho_{a,s,e_1,e_2}(t_0) = |\Psi^{\pm}\rangle\langle\Psi^{\pm}|$, with

$$\begin{aligned} |\Psi^{\pm}\rangle &= \frac{1}{\sqrt{2}}(\hat{a}^{\dagger}_{a,H}\hat{a}^{\dagger}_{s,V} \pm \hat{a}^{\dagger}_{a,V}\hat{a}^{\dagger}_{s,H})|0\rangle_{a,s,e_1,e_2} \\ &\equiv \frac{1}{\sqrt{2}}(|1_h\rangle_a|1_v\rangle_s \pm |1_v\rangle_a|1_h\rangle_s) \otimes |0\rangle_{e_1} \otimes |0\rangle_{e_2}, \end{aligned} \tag{1}$$

where $\hat{a}^{\dagger}_x$ are the photon creation operators on each x-mode. It is worth stressing that due to the possibility of loosing the s-photon during the propagation after its interaction with the e_2-mode, our scheme effectively describes the evolution of a qutrit system (with canonical basis given by the states $|1_h\rangle_s, |1_v\rangle_s$ and $|0\rangle_s$), where information is only stored in the bidimensional subspace associated with one-photon sector.

In our prepared scenario the system-environment interactions are controlled by a series of operations, such as the *BS* one,

$$\begin{aligned} \hat{BS}_{s,e_1} \cdot [|1\rangle_s \otimes |0\rangle_{e_1}] &\rightarrow i\sqrt{r}|1\rangle_s \otimes |0\rangle_{e_1} + \sqrt{1-r}|0\rangle_s \otimes |1\rangle_{e_1}, \\ \hat{BS}_{s,e_1} \cdot [|0\rangle_s \otimes |1\rangle_{e_1}] &\rightarrow i\sqrt{r}|0\rangle_s \otimes |1\rangle_{e_1} + \sqrt{1-r}|1\rangle_s \otimes |0\rangle_{e_1}, \\ \hat{BS}_{s,e_1} \cdot [|0\rangle_s \otimes |0\rangle_{e_1}] &\rightarrow |0\rangle_s \otimes |0\rangle_{e_1}, \end{aligned} \tag{2}$$

with $|1\rangle = (\alpha|1_h\rangle + \beta|1_v\rangle)/\sqrt{|\alpha|^2 + |\beta|^2}$ and r as its reflectivity factor. The wave plates act according to

$$H\hat{W}P_{s,e_1} = \mathbb{I}_s \otimes \sigma^z_{e_1} \text{ and } Q\hat{W}P_{s,e_1} = \sigma^{z/2}_s \otimes \mathbb{I}_{e_1}, \tag{3}$$

with $\sigma^z = |1_h\rangle\langle 1_h| - |1_v\rangle\langle 1_v| + |0\rangle\langle 0|, \sigma^{z/2} = |1_h\rangle\langle 1_h| + i|1_v\rangle\langle 1_v| + |0\rangle\langle 0|$ and $\mathbb{I} = |1_h\rangle\langle 1_h| + |1_v\rangle\langle 1_v| + |0\rangle\langle 0|$.

The attenuation operation applied by the filter F connects the environment space of the remaining light ($\mathcal{H}_{e_1}$) with the space of the absorbed light ($\mathcal{H}_{e_2}$) according to

$$\begin{aligned} \hat{F}_{e_1,e_2} \cdot [|1\rangle_{e_1} \otimes |0\rangle_{e_2}] &\rightarrow \sqrt{T}|1\rangle_{e_1} \otimes |0\rangle_{e_2} + \sqrt{1-T}|0\rangle_{e_1} \otimes |1\rangle_{e_2}, \\ \hat{F}_{e_1,e_2} \cdot [|0\rangle_{e_1} \otimes |1\rangle_{e_2}] &\rightarrow |0\rangle_{e_1} \otimes |1\rangle_{e_2}, \\ \hat{F}_{e_1,e_2} \cdot [|0\rangle_{e_1} \otimes |0\rangle_{e_2}] &\rightarrow |0\rangle_{e_1} \otimes |0\rangle_{e_2}, \end{aligned} \tag{4}$$

which generates the effective inter-environment collisions that can reset the e_1-mode to the vacuum state depending on the absorption factor $1 - T$. Finally the phase control acts as

$$\hat{\theta}_{s,e_1} = |0\rangle_s\langle 0|_s \otimes |0\rangle_{e_1}\langle 0|_{e_1} + |0\rangle_s\langle 0|_s \otimes |1\rangle_{e_1}\langle 1|_{e_1} + e^{i\theta}|1\rangle_s\langle 1|_s \otimes |0\rangle_{e_1}\langle 0|_{e_1}. \tag{5}$$

Then, the super-operator can be written as follows:

$$\varepsilon(t_k, t_{k-1}) = \mathbb{I}_s \otimes \hat{F}_{e_1,e_2} \circ ((\hat{\theta}_{s,e_1} \circ H\hat{W}P_{s,e_1} \circ Q\hat{W}P_{s,e_1} \circ \hat{BS}_{s,e_1}) \otimes \mathbb{I}_{e_2}). \tag{6}$$

According to our CM represented in Fig. 2, the input state $\rho_{a,s,e_1,e_2}(t_0)$ evolves as

$$\rho_{a,s,e_1,e_2}(t_1, t_0) = (\mathbb{I}_a \otimes \varepsilon(t_1, t_0)) \cdot \rho_{a,s,e_1,e_2}(t_0) \cdot (\mathbb{I}_a \otimes \varepsilon(t_1, t_0))^{\dagger}, \tag{7}$$

at the first step of the evolution. For consecutive steps, the process can be repeated with variations on $\varepsilon(t_k, t_{k-1})$ or by using the same operation. Finally, one can extract the ancilla-system state as $\rho_{a,s}(t_k) = Tr_{e_1,e_2}[\rho_{a,s,e_1,e_2}(t_k)]$ or the ancilla-environment state $\rho_{a,e_1}(t_k) = Tr_{s,e_2}[\rho_{a,s,e_1,e_2}(t_k)]$ by tracing out the undesired spaces and measuring bipartite tomographies after the action of the k single step process.

A characterization of the non-Markovianity of the process can then be obtained by studying the evolution of the concurrence $C_{a,s}$ between the ancilla a and the system s at the various steps of the interferometric propagation. From the results of[14,36] we know in fact that in the cases where the relation $C_{a,s}(t_k) > C_{a,s}(t_{k-1})$ holds for some $k > 1$, a back-flow of information from e_1 to s has occurred, resulting in a clear indication of a non-Markovian character of the system dynamics. On the contrary a null increase of $C_{a,s}(t_k)$ cannot be used as an indication of Markovianity.

The magnitude of all information backflows between two steps of the evolution gauges the degree of non-Markovianity, which can be estimated by considering the integral of the concurrence variation[37,38], over the time intervals in which it increases, i.e. the quantity

$$\mathcal{N} = \int_{\dot{C}_{a,s}>0} \dot{C}_{a,s}(t)dt. \tag{8}$$

As already mentioned our system s is intrinsically 3-dimensional. Accordingly the $C_{a,s}$ appearing in Eq. 8 should be the qutrits concurrence[38] instead of the standard qubit one[37]. However, for the sake of simplicity, in the experimental implementation which we present in the following sections, we shall restrict the analysis only to the

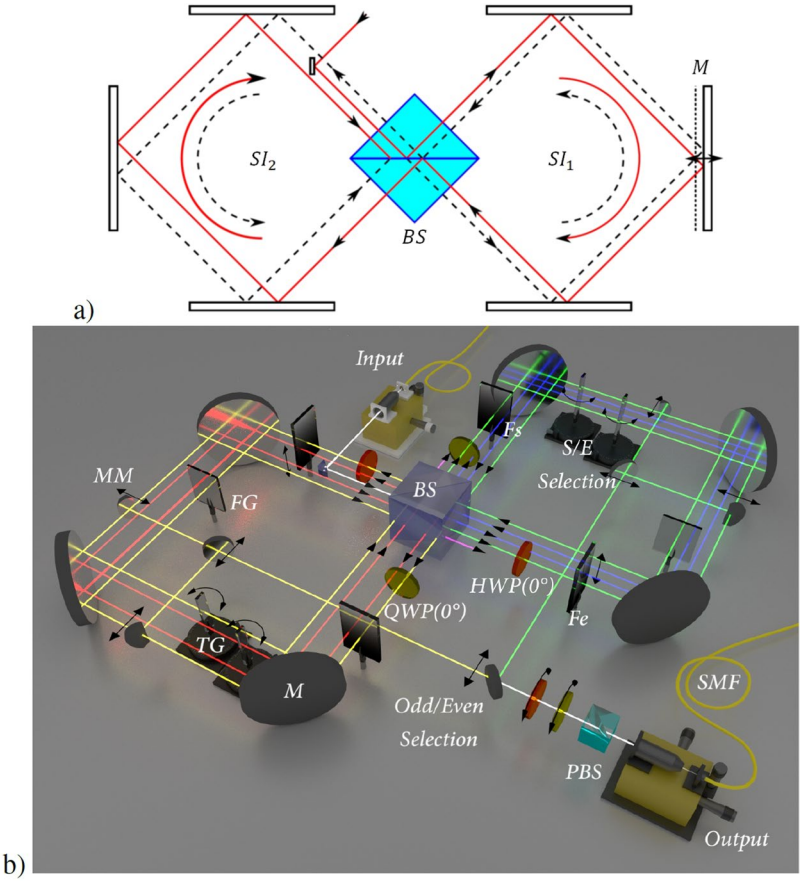

Figure 3. (**a**) Multipass scheme on a double *SI*. The *s*-modes and e-modes circulating in the clockwise and counter-clockwise trajectories inside each *SI*, respectively. (**b**) Complete setup for the collisional model. One can extract $\rho_{a,s}(t_k)$ or $\rho_{a,e}(t_k)$ by selecting the trajectories direction, the odd or even steps by choosing the *SI*, and the step number by using the external *moving mirrors* (*MM*) with translational stages. We use a single filter F^s and a single filter F^e for all odd and even steps. The phase factor θ_k is achieved by the *tilting glass plate* (*TG*) respect to the *fixed glass* (*FG*). Any output qubit can be measured in the tomography stage together with the external ancillary qubit. Here the blue beams correspond to the first step, red beams to second step, the green ones to the third step and yellow ones to the fourth step.

entanglement between the single-photon sectors of *s* and *a*, by property post-selecting our data. Accordingly our measurements do not complete capture the full non-Markovian character implicit in Eq. 8.

Experimental Implementation

The experimental setup is based on two concatenated bulk optics *Sagnac interferometers* (*SIs*) as described in Fig. 3a). They are initially prepared in a collinear configuration, that by applying the displacement of a mirror in SI_1 is transformed in a displaced multipass scheme that replicates the CM of Fig. 2. Here we exploit a geometry endowed with high intrinsic phase stability, where different *BSs* (present in the scheme of Fig. 1) are substituted by different transversal points on a single *BS*. In this scheme the odd steps circulate in SI_1, while the even ones circulate in SI_2. The configuration is equivalent to the model of Fig. 2 since we can choose the s-modes and the e_1-modes as the clockwise and counter-clockwise trajectories inside each *SI*, respectively. For the sake of simplicity, from now on we will use the label "*e*-environment" only for the non absorbed space of the environment, because its complementary part cannot be measured in our configuration.

The relative phase factors θ_k are implemented by a fixed glass plate intersecting all the e-modes inside each *SI*, while thin glass plates are placed in every s-mode and tilted independently (see Fig. 3b). The transmissivity factors $T_k = \frac{T_k^e}{T_k^s}$ are implemented by a single neutral density filter F^e with transmissivity T^e that intersects all the e-modes inside each *SI*, while another filter F^s with transmissivity T^s intersects all the *s*-modes for time-compensation between both optical paths. In this configuration both filters introduce only a controlled absorption, that represents an intrinsic degree of Markovianity under any kind of regime. Even so, the *s*-*e* absorptions can be mapped by the relative absorption factor T_k. Analogously, a single *QWP* intersects all s-modes of each *SI*, while a single *HWP* intersects all the *e*-modes. Since s-mode and *e*-mode contain the same kind of optical elements, we ensure temporally compensated trajectories with an uncertainty of $<30\,\mu m$ per step. The superposition of the 2^k trajectories at step k is collected by a *single-mode optical fiber* (*SMF*) after the tomography stage of *s*-*e* modes. Analogously, another *SMF* collects the external a-mode.

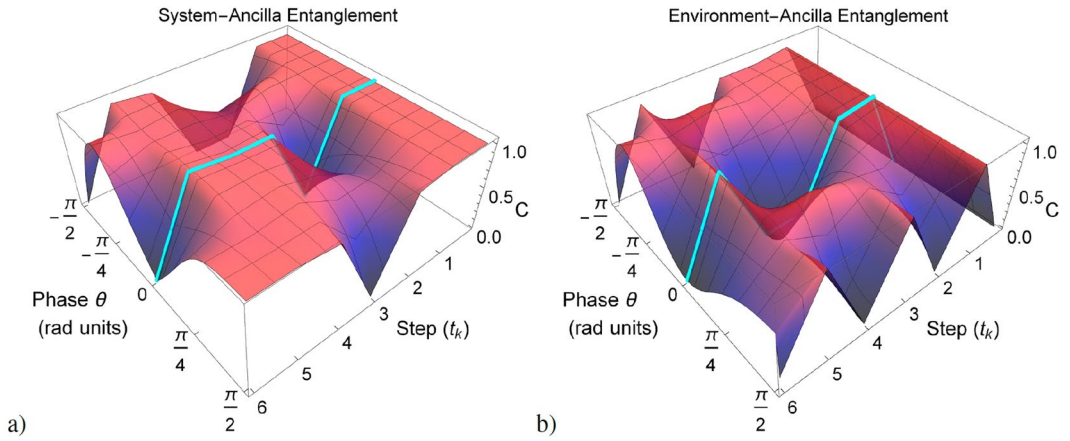

Figure 4. Simulated non-Markovian SE of an ideal Bell input state $|\Psi^{\pm}\rangle$ and ideal optics. Here all the steps are prepared with environment memory parameter $T = 1$ (full non-Markovian regime) and phase difference θ. (**a**) Concurrence for system-ancilla state $\rho_{a,s}(t_k)$. (**b**) Concurrence for environment-ancilla state $\rho_{a,e}(t_k)$.

In this work we focus our attention on the case where all the steps are identical, namely by using a unique filtering factor $T_k = F$ and phase factor $\theta_k = \theta$. This regime can be described by

$$\varepsilon(t_k, t_0) = (\varepsilon(t_1, t_0))^k, \tag{9}$$

and corresponds to the case of a *stroboscopic evolution* (SE)[35].

The entangled state $\rho_{a,s}(t_0) = |\Psi^{\pm}_{a,s}\rangle\langle\Psi^{\pm}_{a,s}|$ is prepared by two indistinguishable processes of Type-II *spontaneous parametric down conversion* (SPDC) inside a high brilliance, high purity Sagnac source based on a *periodically-poled KTP* (PPKTP) non-linear crystal[39]. Here a single-mode continuous-wave laser at 405 *nm* is converted into pairs of photons with orthogonal polarizations at 810 *nm* of wavelength and 0.42 *nm* of line-width (measured by techniques described in[40]). One photon is injected in the *s*-mode of the setup, while the other travels through the external *a*-mode. Finally we reconstruct the post-selected state associated to the single-photon sectors of the density matrices $\rho_{a,s}(t_k)$ or $\rho_{a,e}(t_k)$ by bipartite hyper-complete tomographies between their associated modes (see Fig. 2b).

In Fig. 4 we show a simulation of the possible non-Markovian dynamics under the SE with maximum environment memory ($T = 1$) and variable phase factor θ. These predicted scenarios were obtained by considering an ideal Bell input state $|\Psi^{\pm}\rangle$ and ideal optical elements, e.g. symmetric *BS* and no-losses elements. They are interesting to understand and identify the flows and back-flows of information, which can be used in the analysis of engineered *s*-*e* couplings and its permeability or temporally localized communications for noise avoidance. Besides the *s*-*e* collision, the *e*-mode also suffers inter-environment collisions with the absorption space of the environment. Thus, there is a complex information exchange where it is difficult to identify particular correlations exclusively between both *a*-*s* and *a*-*e* concurrence behaviours.

In Fig. 5 we show a comparison between three SEs considering ideal optical elements, the actual experimental input state $|\Psi\rangle_{exp}$, a phase factor $\theta = \pi/2$ and different degrees of memory T. In the case $T = 1$ it results a fast entanglement fluctuation with a non-Markovian degree of $\mathcal{N} = 0.475$ up to the sixth step. In the case $T = 1/4$ one obtains a slower entanglement fluctuation that gives $\mathcal{N} = 0.185$, while in the case $T = 1/16$ it emerges an even slower fluctuation with $\mathcal{N} = 0.005$ (all values of $\mathcal{N}$ reported here are computed on the post-selected single-photon sectors).

Experimental Results

The experimental test was restricted to the case of a SE with $\theta = 0$ as seen in the light-blue lines of Fig. 4a,b, but considering real optical elements. The prepared entangled state $\Omega_{a,s}$ showed a measured Fidelity $F = |\langle\Psi^{\pm}_{a,s}|\Omega_{a,s}|\Psi^{\pm}_{a,s}\rangle| = 0.9712 \pm 0.0004$, then the simulated data for the imperfect evolution referred to a Werner input mixed state[41–43] $\Omega_{a,s} = \frac{4F-1}{3}|\Psi^{\pm}_{a,s}\rangle\langle\Psi^{\pm}_{a,s}| + \frac{1-F}{3}\mathbb{I}_a \otimes \mathbb{I}_s$.

In Fig. 6 we present the concurrence fluctuations of the single-photon sectors expressed in the post-selected density matrices $\rho_{a,s}(t_k)$ and $\rho_{a,e}(t_k)$ during the SE. These states are reconstructed by normalizing the remaining non absorbed coincident photons, and by consequence the associated concurrence values become invariant under losses. Nevertheless, both dynamics behave according to the simulation for the Werner-like input state $\Omega_{a,s}$. In the case $T = 1$ of Fig. 6a we obtained the highest possible non-Markovianity, where the large concurrence fluctuations give us $\mathcal{N} = 0.3232$. As seen in Fig. 7, in the case $T = 0.209$ we obtained reduced concurrence revivals and non-Markovianity of $\mathcal{N} = 0.1442$, while in the case $T = 0$ we confirmed the lowest possible non-markovianity by obtaining a near to zero value on $\mathcal{N} = 0.0044$.

For our particular CM, these results confirm that entanglement revivals are strictly connected to the environment memory. In fact, they show with high precision that decreasing values on T reduce the information

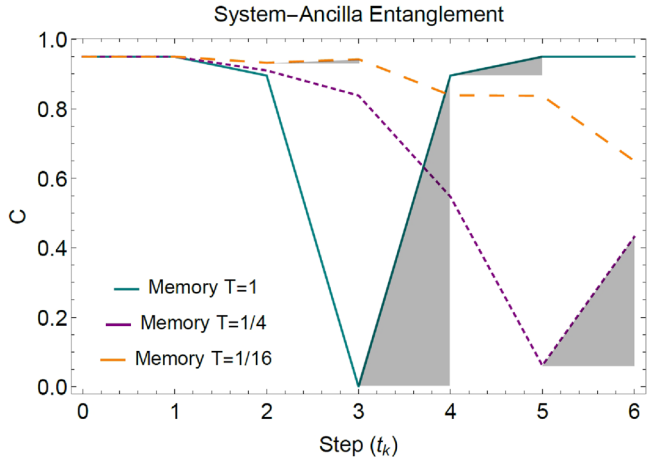

Figure 5. Simulated non-Markovian SE of the experimental input state $|\Psi^{\pm}\rangle_{exp}$ in the case of ideal optics and $\theta = \pi/4$. The area of the grey shaded regions correspond to the integral contributions in the quantifier $\mathcal{N}$. For finite number of steps the entanglement revival is lower at lower values of T.

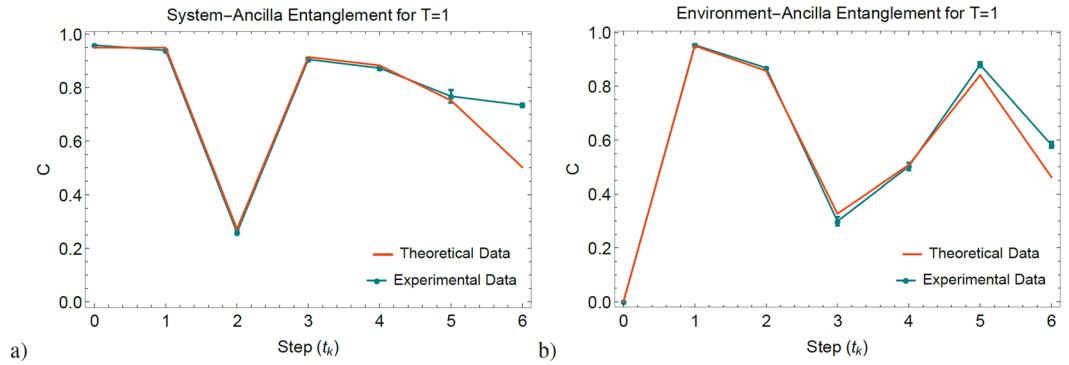

Figure 6. Non-Markovian dynamics with maximum memory ($T = 1$). (**a**) Concurrence of $\rho_{a,s}(t_k)$. (**b**) Concurrence of $\rho_{a,e}(t_k)$. All error bars were calculated from the propagation of 100 Monte-Carlo simulations with Poisson statistics, while theoretical data were simulated by considering the actual optical elements of the interferometric setup.

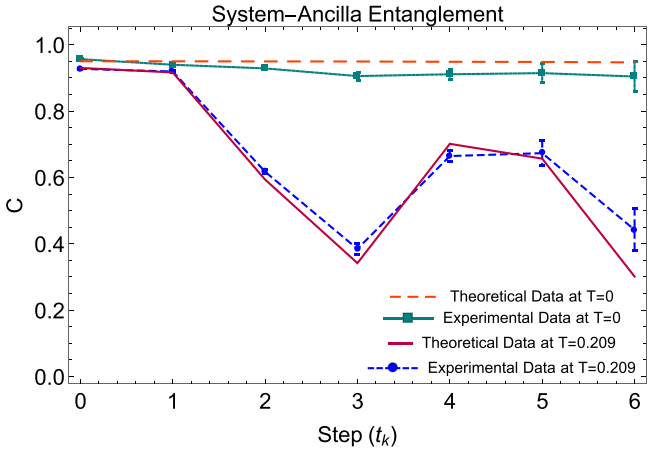

Figure 7. Evolution of Polarization Entanglement with reduced memory ($T = 0$ and $T = 0.209$). Concurrence of the single-photon sectors, post-select density matrix $\rho_{a,s}(t_k)$. All error bars were calculated from the propagation of 100 Monte-Carlo simulations with Poisson statistics, while theoretical data were simulated by considering the actual optical elements of the interferometric setup.

back-flows to the s-mode. The slight deviation from the expected theoretical simulations originates from the not perfect superposition of all possible photon trajectories. Even so, this error is strongly minimized by the use of *SMFs* as final spatial filters.

Conclusions

In this work we presented a linear optics setup that allows to simulate different open quantum systems dynamics. It is based on a novel interferometric structure that guarantees high phase stability and a multipass evolution in a compact setup, that makes possible to study the dynamics up to 6 steps at least. The dynamics studied here represents the first implementation of the so-called *collisional model* for open quantum systems[35], and our results correspond to a particular case of it. The setup is able to simulate a wide variety of stroboscopic evolutions, from strictly Markovian all the way up to strongly non-Markovian dynamics, where quantum memory effects show their contribution. We can experimentally track the role of system-environment and intra-environment interactions in the arising of non-Markovian features and characterize the transition between the two regimes. As the field of quantum technologies spreads, more and more attention has being addressed to the study of non-Markovian dynamics. It can, in principle, be used for efficient information processing[44–48], as well as for engineering novel interesting quantum states[49–51]. In this perspective, our scheme can be of great interest, thanks to its stability, modular nature and direct access to the environmental degrees of freedom.

References

1. Cirac, J. I. & Zoller, P. Quantum computations with cold trapped ions. *Phys. Rev. Lett.* **74**, 4091–4094, https://doi.org/10.1103/PhysRevLett.74.4091 (1995).
2. Loss, D. & DiVincenzo, D. P. Quantum computation with quantum dots. *Phys. Rev. A* **57**, 120–126, https://doi.org/10.1103/PhysRevA.57.120 (1998).
3. Orieux, A. *et al*. Experimental on-demand recovery of entanglement by local operations within non-markovian dynamics. *Scientific reports* **5**, 8575 (2015).
4. Liu, B.-H. *et al*. Experimental control of the transition from markovian to non-markovian dynamics of open quantum systems. *Nature Physics* **7**, 931 (2011).
5. Zou, C.-L. *et al*. Photonic simulation of system-environment interaction: Non-markovian processes and dynamical decoupling. *Phys. Rev. A* **88**, 063806, https://doi.org/10.1103/PhysRevA.88.063806 (2013).
6. Liu, Z.-D. *et al*. Experimental implementation of fully controlled dephasing dynamics and synthetic spectral densities. *Nature Communications* **9**, 3453, https://doi.org/10.1038/s41467-018-05817-x (2018).
7. de Vega, I. & Alonso, D. Dynamics of non-markovian open quantum systems. *Rev. Mod. Phys.* **89**, 015001, https://doi.org/10.1103/RevModPhys.89.015001 (2017).
8. Rosario, A., Massoni, E. & Zela, F. D. On the relationship between non-markovianity and entanglement protection. *Journal of Physics B: Atomic, Molecular and Optical Physics* **45**, 095501, http://stacks.iop.org/0953-4075/45/i=9/a=095501 (2012).
9. Terhal, B. M. & Burkard, G. Fault-tolerant quantum computation for local non-markovian noise. *Phys. Rev. A* **71**, 012336, https://doi.org/10.1103/PhysRevA.71.012336 (2005).
10. Tang, J.-S. *et al*. Measuring non-markovianity of processes with controllable system-environment interaction. *EPL* (*Europhysics Letters*) **97**, 10002, http://stacks.iop.org/0295-5075/97/i=1/a=10002 (2012).
11. Liu, B.-H. *et al*. Photonic realization of nonlocal memory effects and non-markovian quantum probes. *Sci Rep* **3**, 1781, http://www.ncbi.nlm.nih.gov/pmc/articles/PMC3646274/ (2013).
12. Chruściński, D. & Kossakowski, A. Witnessing non-markovianity of quantum evolution. *The European Physical Journal D* **68**, 7, https://doi.org/10.1140/epjd/e2013-40171-9 (2014).
13. Addis, C., Bylicka, B., Chruściński, D. & Maniscalco, S. Comparative study of non-markovianity measures in exactly solvable one- and two-qubit models. *Phys. Rev. A* **90**, 052103, https://doi.org/10.1103/PhysRevA.90.052103 (2014).
14. Rivas, A., Huelga, S. F. & Plenio, M. B. Quantum non-markovianity: characterization, quantification and detection. *Reports on Progress in Physics* **77**, 094001, http://stacks.iop.org/0034-4885/77/i=9/a=094001 (2014).
15. Breuer, H.-P., Laine, E.-M., Piilo, J. & Vacchini, B. Colloquium: Non-markovian dynamics in open quantum systems. *Rev. Mod. Phys.* **88**, 021002, https://doi.org/10.1103/RevModPhys.88.021002 (2016).
16. Breuer, H.-P., Laine, E.-M. & Piilo, J. Measure for the degree of non-markovian behavior of quantum processes in open systems. *Phys. Rev. Lett.* **103**, 210401, https://doi.org/10.1103/PhysRevLett.103.210401 (2009).
17. Laine, E.-M., Piilo, J. & Breuer, H.-P. Measure for the non-markovianity of quantum processes. *Phys. Rev. A* **81**, 062115, https://doi.org/10.1103/PhysRevA.81.062115 (2010).
18. Fanchini, F. F. *et al*. Non-markovianity through accessible information. *Phys. Rev. Lett.* **112**, 210402, https://doi.org/10.1103/PhysRevLett.112.210402 (2014).
19. Chruściński, D., Macchiavello, C. & Maniscalco, S. Detecting non-markovianity of quantum evolution via spectra of dynamical maps. *Phys. Rev. Lett.* **118**, 080404, https://doi.org/10.1103/PhysRevLett.118.080404 (2017).
20. Bellomo, B., Pasquale, A. D., Gualdi, G. & Marzolino, U. A tomographic approach to non-markovian master equations. *Journal of Physics A: Mathematical and Theoretical* **43**, 395303, http://stacks.iop.org/1751-8121/43/i=39/a=395303 (2010).
21. Rivas, A., Huelga, S. F. & Plenio, M. B. Entanglement and non-markovianity of quantum evolutions. *Phys. Rev. Lett.* **105**, 050403, https://doi.org/10.1103/PhysRevLett.105.050403 (2010).
22. Rau, J. Relaxation phenomena in spin and harmonic oscillator systems. *Phys. Rev.* **129**, 1880–1888, https://doi.org/10.1103/PhysRev.129.1880 (1963).
23. Ziman, M. *et al*. Diluting quantum information: An analysis of information transfer in system-reservoir interactions. *Phys. Rev. A* **65**, 042105, https://doi.org/10.1103/PhysRevA.65.042105 (2002).
24. Vacchini, B. General structure of quantum collisional models. *International Journal of Quantum Information* **12**, 1461011, https://doi.org/10.1142/S0219749914610115 (2014).
25. Lorenzo, S., Ciccarello, F. & Palma, G. M. Composite quantum collision models. *Phys. Rev. A* **96**, 032107, https://doi.org/10.1103/PhysRevA.96.032107 (2017).
26. Bernardes, N. K., Carvalho, A. R. R., Monken, C. H. & Santos, M. F. Environmental correlations and markovian to non-markovian transitions in collisional models. *Phys. Rev. A* **90**, 032111, https://doi.org/10.1103/PhysRevA.90.032111 (2014).
27. McCloskey, R. & Paternostro, M. Non-markovianity and system-environment correlations in a microscopic collision model. *Phys. Rev. A* **89**, 052120, https://doi.org/10.1103/PhysRevA.89.052120 (2014).
28. Bodor, A., Diósi, L., Kallus, Z. & Konrad, T. Structural features of non-markovian open quantum systems using quantum chains. *Phys. Rev. A* **87**, 052113, https://doi.org/10.1103/PhysRevA.87.052113 (2013).
29. Ciccarello, F., Palma, G. M. & Giovannetti, V. Collision-model-based approach to non-markovian quantum dynamics. *Phys. Rev. A* **87**, 040103, https://doi.org/10.1103/PhysRevA.87.040103 (2013).

30. Ciccarello, F. & Giovannetti, V. A quantum non-markovian collision model: incoherent swap case. *Physica Scripta* **2013**, 014010, http://stacks.iop.org/1402-4896/2013/i=T153/a=014010 (2013).
31. Rybár, T., Filippov, S. N., Ziman, M. & Bužek, V. Simulation of indivisible qubit channels in collision models. *Journal of Physics B: Atomic, Molecular and Optical Physics* **45**, 154006, http://stacks.iop.org/0953-4075/45/i=15/a=154006 (2012).
32. Jin, J. & Shui Yu, C. Non-markovianity in the collision model with environmental block. *New Journal of Physics* **20**, *053026*, http://stacks.iop.org/1367-2630/20/i=5/a=053026 (2018).
33. Chiuri, A., Greganti, C., Mazzola, L., Paternostro, M. & Mataloni, P. Linear optics simulation of quantum non-markovian dynamics. *Scientific reports* **2**, 968 (2012).
34. Ciccarello, F. *Quantum Measurements and Quantum Metrology*, vol. 4, chap. Collision models in quantum optics, 53, https://www.degruyter.com/view/j/qmetro.2017.4.issue-1/qmetro-2017-0007/qmetro-2017-0007.xml, 1 (2017).
35. Jin, J. *et al*. All-optical non-markovian stroboscopic quantum simulator. *Phys. Rev. A* **91**, 012122, https://doi.org/10.1103/PhysRevA.91.012122 (2015).
36. Lorenzo, S., Plastina, F. & Paternostro, M. Geometrical characterization of non-markovianity. *Phys. Rev. A* **88**, 020102, https://doi.org/10.1103/PhysRevA.88.020102 (2013).
37. Wootters, W. K. Entanglement of formation of an arbitrary state of two qubits. *Phys. Rev. Lett.* **80**, 2245–2248, https://doi.org/10.1103/PhysRevLett.80.2245 (1998).
38. Herreño-Fierro, C. & Luthra, J. R. Generalized concurrence and limits of separability for two qutrits. *eprint arXiv:quantph/0507223*, https://arxiv.org/abs/quant-ph/0507223 (2005).
39. Fedrizzi, A., Herbst, T., Poppe, A., Jennewein, T. & Zeilinger, A. A wavelength-tunable fiber-coupled source of narrowband entangled photons. *Opt. Express* **15**, 15377–15386, http://www.opticsexpress.org/abstract.cfm?URI=oe-15-23-15377 (2007).
40. Cuevas, Á. *et al*. First observation of the quantized exciton-polariton field and effect of interactions on a single polariton. *Science Advances* **4**, http://advances.sciencemag.org/content/4/4/eaao6814, http://advances.sciencemag.org/content/4/4/eaao6814.full.pdf (2018).
41. Hiroshima, T. & Ishizaka, S. Local and nonlocal properties of werner states. *Phys. Rev. A* **62**, 044302, https://doi.org/10.1103/PhysRevA.62.044302 (2000).
42. Barbieri, M., De Martini, F., Di Nepi, G. & Mataloni, P. Generation and characterization of werner states and maximally entangled mixed states by a universal source of entanglement. *Phys. Rev. Lett.* **92**, 177901, https://doi.org/10.1103/PhysRevLett.92.177901 (2004).
43. Cuevas, A. *et al*. Experimental detection of quantum channel capacities. *Phys. Rev. Lett.* **119**, 100502, https://doi.org/10.1103/PhysRevLett.119.100502 (2017).
44. Plenio, M. B. & Huelga, S. F. Dephasing-assisted transport: quantum networks and biomolecules. *New Journal of Physics* **10**, 113019, http://stacks.iop.org/1367-2630/10/i=11/a=113019 (2008).
45. Caruso, F., Chin, A. W., Datta, A., Huelga, S. F. & Plenio, M. B. Highly efficient energy excitation transfer in light-harvesting complexes: The fundamental role of noise-assisted transport. *The Journal of Chemical Physics* **131**, 105106, https://doi.org/10.1063/1.3223548 (2009).
46. Viola, L. & Lloyd, S. Dynamical suppression of decoherence in two-state quantum systems. *Phys. Rev. A* **58**, 2733–2744, https://doi.org/10.1103/PhysRevA.58.2733 (1998).
47. Liu, B.-H. *et al*. Efficient superdense coding in the presence of non-markovian noise. *EPL (Europhysics Letters)* **114**, 10005 (2016).
48. Dong, Y. *et al*. Non-markovianity-assisted high-fidelity deutsch–jozsa algorithm in diamond. *npj Quantum Information* **4**, 3 (2018).
49. Huelga, S. F., Rivas, A. & Plenio, M. B. Non-markovianity-assisted steady state entanglement. *Phys. Rev. Lett.* **108**, 160402, https://doi.org/10.1103/PhysRevLett.108.160402 (2012).
50. Plenio, M. B. & Huelga, S. F. Entangled light from white noise. *Phys. Rev. Lett.* **88**, 197901, https://doi.org/10.1103/PhysRevLett.88.197901 (2002).
51. Kraus, B. *et al*. Preparation of entangled states by quantum markov processes. *Phys. Rev. A* **78**, 042307, https://doi.org/10.1103/PhysRevA.78.042307 (2008).
52. White, A. G., James, D. F. V., Eberhard, P. H. & Kwiat, P. G. Nonmaximally entangled states: Production, characterization, and utilization. *Phys. Rev. Lett.* **83**, 3103–3107, https://doi.org/10.1103/PhysRevLett.83.3103 (1999).

Acknowledgements

We acknowledge support from the European Commission grants FP7-ICT-2011-9-600838 (QWAD - Quantum Waveguides Application and Development) and H2020-FETPROACT-2014 (QUCHIP - Quantum Simulation on a Photonic Chip). We thank partial support from the Chilean agency Comisión Nacional de Investigación Científica y Tecnológica (CONICYT) and its Ph.D. scholarships "Becas Chile".

Author Contributions

V.G. and P.M. proposed the theoretical frame and the optical scheme presented in Fig. 2, Á.C. proposed and coordinated the experimental multipass implementation, A.G., C.L. and L.D.B. achieved and analysed the experimental measures, A.D.P. and F.S. contributed to the interpretation of results. All authors contributed to the writing of the manuscript.

Additional Information

Competing Interests: The authors declare no competing interests.

Publisher's note: Springer Nature remains neutral with regard to jurisdictional claims in published maps and institutional affiliations.

Open Access This article is licensed under a Creative Commons Attribution 4.0 International License, which permits use, sharing, adaptation, distribution and reproduction in any medium or format, as long as you give appropriate credit to the original author(s) and the source, provide a link to the Creative Commons license, and indicate if changes were made. The images or other third party material in this article are included in the article's Creative Commons license, unless indicated otherwise in a credit line to the material. If material is not included in the article's Creative Commons license and your intended use is not permitted by statutory regulation or exceeds the permitted use, you will need to obtain permission directly from the copyright holder. To view a copy of this license, visit http://creativecommons.org/licenses/by/4.0/.

© The Author(s) 2019